Available online at www.sciencedirect.com

ScienceDirect

IFAC PapersOnline CONFERENCE PAPER ARCHIVE

IFAC PapersOnLine 52-26 (2019) 38–44

Impact of changing cell-cell communication network in models of epithelial pattern formation ⋆

Pedro L. Varela * **Pedro T. Monteiro** ** **Claudine Chaouiya** ***

* *INESC-ID / Instituto Superior Técnico, Univ de Lisboa, Lisboa, PT*
Instituto Gulbenkian de Ciência, Oeiras, PT
** *INESC-ID / Instituto Superior Técnico, Univ de Lisboa, Lisboa, PT*
*** *Aix Marseille Univ, CNRS, Centrale Marseille, I2M, Marseille, FR*
Instituto Gulbenkian de Ciência, Oeiras, PT

Abstract: When modelling multi-cellular systems, one has to account for cell-cell signalling in addition to the molecular networks driving cell behaviours. Here, we aim at exploring how the topology of the cell-cell communication network impacts the behaviour of the whole multi-cellular system. More precisely, we focus on epithelial pattern formation, on which our question can be rephrased in terms of cell sizes and shapes. Relying on a logical modelling framework, and using a simple lateral inhibition model over a population of epithelial cells, we assess the model behaviours considering a variety of communication networks. This study suggests that reasonable deviations from a fixed grid (with regular hexagonal shaped cells) do not change much the resulting patterns. We further explore the impact of cell shapes and show that characteristics such as network regularity and number of shared neighbours of contacting cells are relevant to qualify such deviations.

Keywords: Boolean modelling, Signalling networks, Multi-cellular biological systems, Lateral-inhibition, Pattern generation, Communication networks, Finite automata.

1. INTRODUCTION

Logical modelling (Abou-Jaoudé et al., 2016) has shown to be useful in handling regulatory networks involved in pattern formation in the course of tissue development (Albert and Othmer, 2003; Sánchez et al., 2008; Azpeitia et al., 2010; Fauré et al., 2014). This qualitative framework allows to consider large regulatory networks for which detailed quantitative data are lacking. Logical models account for essential dynamical properties such as model attractors, which can be generally associated with different cell types displaying distinct patterns of gene expression. We have recently released EpiLog, a software tool implementing a hierarchical extension of the logical framework to account for cell-cell communication within a simple epithelium (Varela et al., 2018b). EpiLog defines a cellular automaton over a 2D hexagonal grid, *i.e.*, a grid of hexagons), in which each cell carries its own logical regulatory model.

Specific mechanisms govern the observed regular organisation of epithelia (*e.g.* Vetter et al. (2019)). In EpiLog, the underlying cell communication network is a fixed hexagonal grid, which convey the predominant hexagonal shape of the cells (Gibson et al., 2006). Here, we aim at exploring the implications of EpiLog communication network. To this end, we consider alternative networks diverging from that of the hexagonal grid. To uncover the impact of the topology of the communication network on the induced pattern, we selected a simple model of lateral inhibition, known to drive a precise salt-and-pepper patterning (Collier et al., 1996).

For convenience, and because of our case study, this introduction is restricted to Boolean models, in contrast to multi-valued models in which variables can take more discrete values.

This paper is organised as follows. The background Section 2 provides a brief overview of the modelling framework for cellular and multi-cellular systems, as well as an introduction to the lateral inhibition model. Section 3 introduces the selected communication networks and associated characteristics considered in this study. Section 4 presents the methods used to generate the different communication networks and to simulate the lateral-inhibition model over those networks, getting the reached stable patterns. Section 5 presents the results, which are discussed together with some prospects in Section 6.

2. BACKGROUND

2.1 Boolean modelling

A Boolean model of a regulatory network defines a set of discrete variables x taking their values in $\{0, 1\}$, where the value of x conveys the state of the corresponding regulatory component g_x (active or not, expressed or not, etc.). A Boolean function f_x defines the evolution

⋆ This work was supported by national funds through Fundação para a Ciência e a Tecnologia (FCT) with references UID/CEC/50021/2019 (INESC-ID multi-annual funding) and projects PTDC/BEX-BCB/0772/2014 and PTDC/EEI-CTP/2914/2014.

2405-8963
Peer review under responsibility of International Federation of Automatic Control.
10.1016/j.ifacol.2019.12.233

of the variable x, *i.e.*, the value of x depending on the state of the model (more precisely on the states of the components regulating g_x). Indeed, the function f_x reflects the regulatory structure of g_x (its regulators and their effects on g_x).

A transition function is thus defined: given any state $X = (x_1, \ldots, x_n)$ of the model, $F(X) = (f_{x_1}, \ldots, f_{x_n})$ defines its target state. In a deterministic, synchronous update, $F(X)$ is the successor of X. However, as this updating scheme is often biologically unrealistic, it is preferable to consider the non-deterministic asynchronous update for which at most one variable is updated at each simulation step, each successor differing from X by exactly one component.

A cellular model relates to the regulatory network controlling a specific cellular process. Input components accounting for signals from the micro-environment have no regulation and are associated to constant variables (*i.e.*, $f_x(X) = x$).

2.2 Boolean modelling of multi-cellular systems & EpiLog

To handle multi-cellular systems in which cell-cell communication matters, we proposed to compose cellular models through their input components (see Chaouiya et al. (2013); Varela et al. (2018a) for further detail on this composition). Basically, cell-cell communication operates through signalling proteins that activate receptors of neighbouring cells. For each cell, the neighbouring cells are those connected to the cell through an edge in the underlying communication network.

A multi-cellular model is defined by a collection of as many cellular models as the number of cells, the communication network defining the neighbours of each cell (*i.e.*, cells enabled to send signals to that cell) and, for each input component, an integration function that defines which signals and from how many neighbouring cells (expressed by a *cardinality constraint* of the type $ATLc$, *i.e.*, at least c) should send the signal to activate that input. Here, we focus on juxtacrine signals, *i.e.*, signalling between contacting cells, *i.e.,* that are connected in the communication network.

EpiLog (`http://epilog-tool.org`) is a software tool implementing this framework in the form of cellular automata restricted to 2D hexagonal grids (Varela et al., 2018b). Hexagonal grids have cylindrical or toroidal periodic conditions or not. Hence the sole communication network handled in EpiLog is a regular grid with degree 6 (except possibly at the grid borders). The purpose of this work is to assess to what extent this topological restriction is acceptable.

The default updating scheme in EpiLog is the synchronous one, where all the cellular components in all the cells are simultaneously updated. However, EpiLog allows to associate (synchronous) priority classes with the cellular components and to specify an α-asynchronous update over the cells (Fatès, 2013). This consists in overcoming the classical synchronous update of cellular automata by defining α, the common updating probability of the cells. The resulting update is synchronous when $\alpha = 1$ and, by convention, when $\alpha = 0$ the update is equivalent to the random asynchronous (a unique cell is updated at each simulation step, selecting a single trajectory among all the possible asynchronous behaviours) (Varela et al., 2018b). Finally within a simulation step, when updating a cell, its input nodes are updated first, according to the values of components in neighbouring cells and only then their targets are updated.

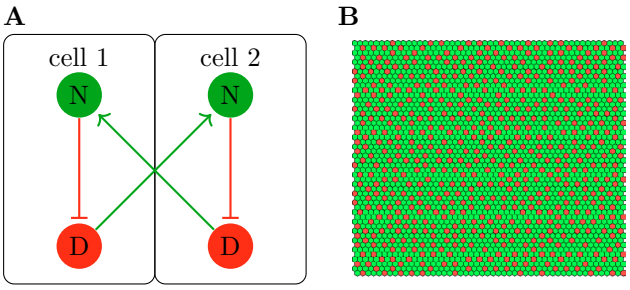

Fig. 1. Simplified Boolean model of lateral inhibition: (A) Two cell model, with cellular networks connected through N (Notch) activation from D (Delta) in the contacting cell. (B) Resulting pattern for the same model over a grid of 50×50 hexagonal cells, considering that N is activated provided D is active in at-least 1 ($ALT1$) contacting cell; green (resp. red) cells are N (resp. D) positive cells.

2.3 Lateral inhibition model

A simplified version of the Delta-Notch signalling system was chosen for the purpose of this study (Collier et al., 1996). This system is well-known for establishing distinct fates of contacting cells through a lateral inhibition mechanism: Notch signalling is initiated when Delta ligand binds to the Notch receptor expressed on a contacting cell, causing its cleavage and the release of the Notch intracellular domain. This then moves into the nucleus where it represses Delta production. The Boolean model of this system is illustrated in Figure 1.

This model is convenient to assess the influence of the communication network topology because it gives rise to archetypal patterns that can be characterised by a simple measure of the cell-type ratio, here assessed as the percentage of Notch expressing cells (see *e.g.* Matsuda et al. (2015)). Hereinafter, cells in which Notch is active (resp. inactive) and Delta is inactive (resp. active) are referred to as N (resp. D) positive cells.

Diverse mathematical models have been delineated to study patterns generated by the Delta-Notch signalling system (see *e.g.* Collier et al. (1996); Ghosh and Tomlin (2004); Palau-Ortin et al. (2015); Tonello and Siebert (2019)). In particular, in Tonello and Siebert (2019), prove that for their Boolean model, under the random asynchronous update, all the attractors are stable states (*i.e.*, there are no stable oscillatory behaviours, and the model will eventually reach a stable pattern), and that all the attractors are reachable from any homogeneous initial configuration in which all the cells have the same state.

3. COMMUNICATION NETWORKS

This section presents a selection of network classes, from regular grids to variations of regular networks and non-

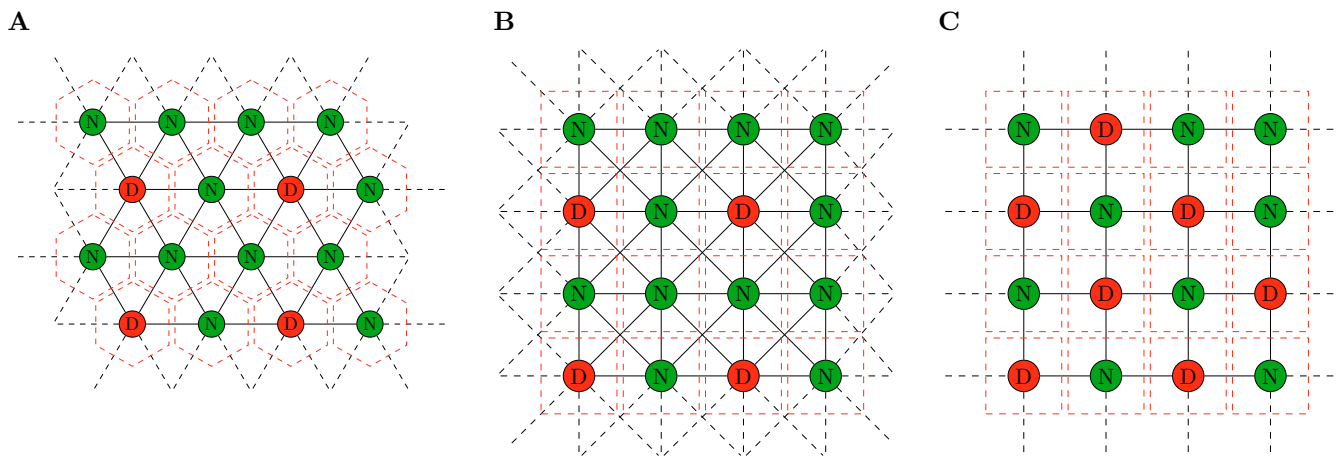

Fig. 2. Communication networks for 4×4 regular grids ($k \in \{4, 6, 8\}$) with toroidal periodic conditions, displaying possible stable patterns for a cardinality constraint $ATL1$. A) Hexagonal grid. B) Square grid with Moore neighbourhood. C) Square grid with von Neumann neighbourhood.

regular ones. We then introduce a few network characteristics considered along this study.

3.1 Network classes

In what follows, we denote by n, the number of nodes (or cells) in the communication network.

Regular grids (RG) are defined by cells with a unique shape (hexagonal or square) placed on a 2D torus. They correspond to regular networks subject to a geometrical constraint (*i.e.*, 2D lattices), with degree $k = 4$ (square cells with a von Neumann neighbourhood), $k = 6$ (hexagonal cells), or $k = 8$ (square cells with a Moore neighbourhood). See Figure 2 for an illustration. Note that, being a 2D torus and due to the hexagonal structure ($k = 6$), dimensions of the grid must be even.

Random regular (RR) networks are such that all their n nodes have the same specified degree k (Steger and Wormald, 1999). Note that $n \times k$ must be even and $k < n$.

Watts-Strogatz (WG) networks are obtained from a regular network with nodes distributed over a ring, each being connected to its k nearest neighbours and then by rewiring the edges given a probability p (Watts and Strogatz, 1998; Barrat and Weigt, 2000). Varying p, nodes in the obtained networks – so-called "small-world" – have a mean degree $\bar{k}$, and at least $k/2$ neighbours. Networks obtained with a probability p are henceforth denoted WGp.

Erdös-Rényi (ER) networks are also associated with a parameter p specifying the probability for a pair of nodes to be connected, the mean degree being $\bar{k} = (n-1) \times p$.

3.2 Network measures and characteristics

Notation:

- A network (V, E) is defined by a set of nodes V, and a set of edges $E \subseteq V \times V$;
- A node degree is denoted by $deg(v) = \#\{w \in V, (v, w) \in E\}$.

Network regularity: among the considered network classes, we can distinguish between those which are regular, where all the nodes have the exact same degree, and those which are non-regular, with node degrees following a given distribution. Figure 3-A shows the degree distribution of the three non-regular networks considered in this work.

Network connectedness: all networks (RG, RR, and WG) but the Erdös-Rényi are connected.

Number of shared neighbours: Given two adjacent nodes v and w, $S(v, w)$ denotes the number of neighbours shared by v and w:

$$S(v, w) = \#\{z \in V, (v, z) \in E \wedge (w, z) \in E\}.$$

Czekanowski-Dice dissimilarity measure: This classical measure applies to pairs of nodes v and w and accounts for the numbers of shared neighbours and the numbers of nodes exclusively connected to v or to w (Angelelli et al., 2008). Here, we only consider the Czekanowski-Dice dissimilarity measure for pairs of connected nodes v and w ($(v, w) \in E$), given by:

$$D(v, w) = \frac{deg(v) + deg(w) - 2(S(v, w) + 1)}{2 + deg(v) + deg(w)}.$$

Hence, the higher the number of shared neighbours, the lower the dissimilarity. In particular, if two nodes have the same neighbours, their dissimilarity measure is zero. In the context of cell communication networks, this corresponds to a situation where two cells are subject to exactly the same signals from their (shared) neighbours, and will thus adopt the same fate.

Note that both shared neighbours and dissimilarity measures are relevant and can be compared for all connected networks, *i.e.,* all except ER (see Table 1). For regular networks, given a degree k, the number of connected pairs of nodes is exactly $k \times n/2$, whereas for non-regular networks this is the mean number of connected nodes.

All pairs of connected nodes in the RG network with $k = 6$ have exactly 2 shared neighbours. As shown in Figure 3-B, we computed the numbers of shared neighbours for the WS

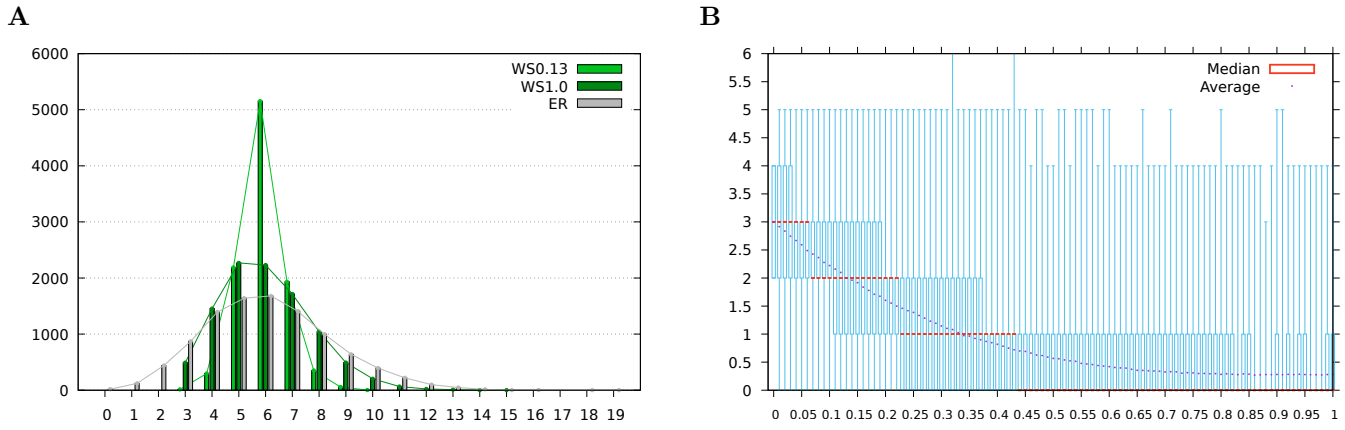

Fig. 3. A) Degree distribution of 10 000 nodes for each non-regular network class, with average degree $\bar{k} = 6$ (100 networks of each class, each network having 100 nodes). B) Distribution of the numbers of shared neighbours in 100 Watts-Strogatz networks, for each $p \in \{0.0, 0.01, \ldots, 1.0\}$. The whisker plot with min, Q1, Q2, Q3 and max values is shown in blue, median (Q2) values highlighted in red and average values in purple.

Table 1. Sets of values for S (shared neighbours) and D (dissimilarity) of pairs of connected nodes

Network	$\mathbf{S(v,w)}$	$\mathbf{D(v,w)}$
Hexagonal grid ($k = 6$)	$\{2\}$	$\{3/7\}$
Square grid ($k = 4$)	$\{0\}$	$\{3/5\}$
Square grid ($k = 8$)	$\{2, 4\}$	$\{5/9\}$
Random regular ($k = 6$)	$\{0, \ldots, 5\}$	$\{i/7\}_{i=0,\ldots,5}$
Watts-Strogatz ($p = 0, k = 6$)	$\{2, 3, 4\}$	$\{i/7\}_{i=1,2,3}$
Watts-Strogatz ($p = 1, \bar{k} = 6$)	$\{0, \ldots, n-2\}$	$[1/2, 1[$

network with $\bar{k} = 6$, for probability $p \in \{0.0, 0.01, \ldots, 1.0\}$. Because the WS network with $p = 0.13$ (denoted WS0.13) has 2 shared neighbours on average, we retained this specific network for comparisons in Section 5.

4. METHODS

The generation of the Random regular (RR), Watts-Strogatz (WS) and Erdös-Rényi (ER) networks was performed using the NetworkX 2.2 (`https://networkx.github.io/`) Python software package (Hagberg et al., 2008). The Regular grid (RG) was generated using our own Python script. Section 7 provides the location of all the scripts of network generation and analyses, as well as for simulations and pattern analyses.

For each network class and each parameter combination (see Table 2), we generated 100 communication networks. Note that for the RG, only one network was generated for each degree, which defines a unique network.

Table 2. Network generation parameters.

Network	Size n	Degree $\bar{k}$	Probability p
Regular grid	100	$\{4, 6, 8\}$	N/A
Random regular	100	$\{4, 6, 8\}$	N/A
Watts-Strogatz	100	$\{4, 6, 8\}$	$\{0.0, 0.01, \ldots, 1.0\}$
Erdös-Rényi	100	$\{4, 6, 8\}$	$\{\bar{k}/n\}$

Network statistics, such as degree distribution or number of shared neighbours, are retrieved immediately after each network generation using a Python script.

To carry out all the simulations, we used a modified version of EpiLog that permits to load a predefined communication network. For each communication network (100 instances for all classes but the RG), 100 simulations were performed. For each instance of the RG, 10 000 simulations were done. All simulations were carried out under a synchronous update within cells, a random asynchronous update ($\alpha = 0$) between cells, and started from the naive initial state, in which all the components are set to value 0. This is because all the stable patterns are reachable from this homogeneous initial state (Tonello and Siebert, 2019).

EpiLog creates a file for each stable pattern reached. Then a Python script retrieves the percentage of N positive cells from these files.

5. RESULTS

Considering the different classes of communication networks described above, we evaluated how the stable patterns of the lateral-inhibition model change depending on different parameters. Patterns are characterised by the percentages of N positive cells.

5.1 Network regularity and cardinality constraints

In this section, the (mean) degree of all the nodes in all the networks is fixed to 6. The cardinality constraint varies from $ATL1$ to $ATL6$.

Increased cardinality constraint means that more neighbouring D positive cells (*i.e.*, connected in the communication network) are required to get a N positive cell (*i.e.*. As illustrated in the Figure 4-A for the regular hexagonal grid, the percentage of N positive cells (green) in the reached stable pattern decreases with the increase of the cardinality constraint. This decrease is exactly compensated by the emergence of D positive cells. Figure 4-B shows that for all the communications networks, varying the cardinality constraint ($ATLc$ for $c \in \{1, \ldots, 6\}$) results in a decrease of the average percentages of N positive cells in the resulting stable patterns.

Moreover, as illustrated in Figure 5, for all the regular networks, the percentages of N positive cells for the cardinality constrains $ATLc$ and $ATL6{-}c{+}1$ (for $c \in \{1, 2, 3\}$) add

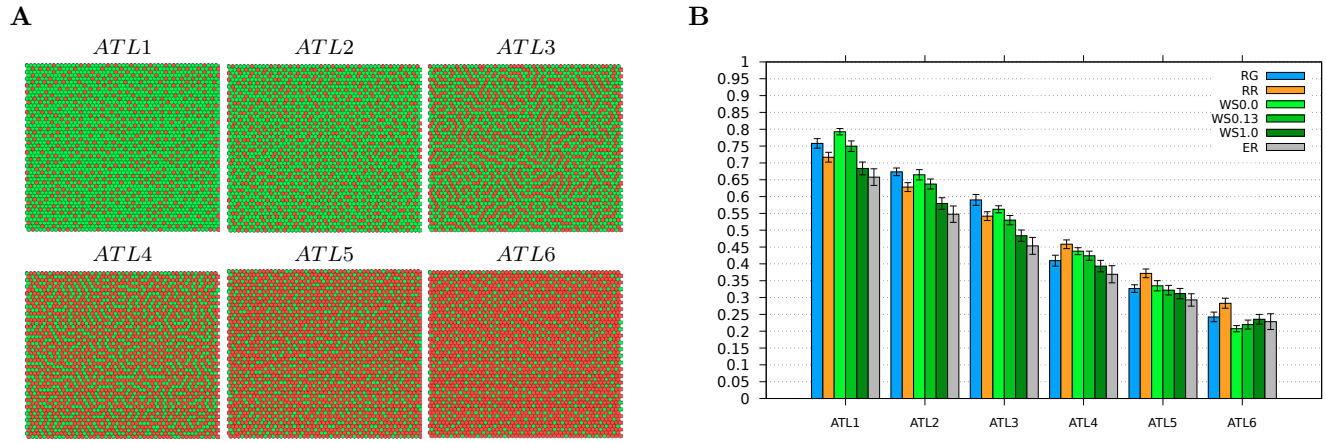

Fig. 4. Percentages of N positive cells when varying the cardinality constraint $ATLc$, $c = 1, \ldots, 6$: A) Resulting patterns for the same 50×50 regular hexagonal grid ($k = 6$); B) Average percentages for the different network classes ($\bar{k} = 6$).

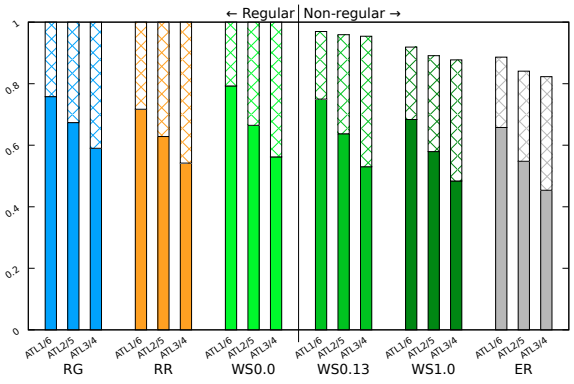

Fig. 5. Stacked histogram showing the complementarity of N percentages ($\bar{k} = 6$). The lower plain bars indicate N percentages for $ATLc$, whereas the upper bars indicate the N percentages for $ATLc - 6 + 1$.

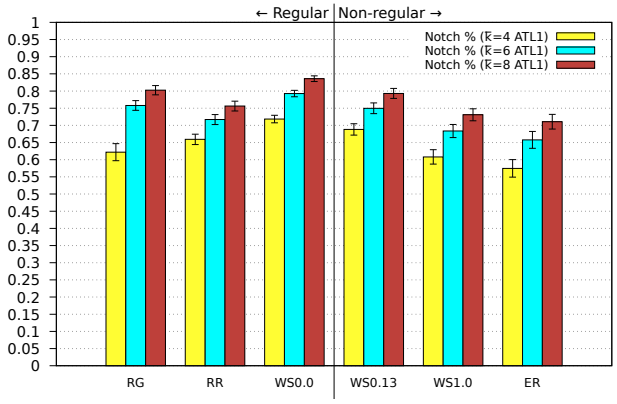

Fig. 6. Average percentages of N positive cells for degrees $\bar{k} \in \{4, 6, 8\}$, for different network classes, a cardinality constraint fixed to $ATL1$; Regular Grid (RG), Random Regular (RR), Watts-Strogatz with rewiring probability p (WSp), Erdös-Rényi (ER).

up to 100%. In other words, the percentage of N positive cells for $ATLc$ equals the percentage of D positive cells for $ATL6 - c + 1$. This property could be easily proved for any regular communication network. However, this property does not hold for the non-regular networks. Indeed, cells with less than c neighbours, eventually become D positive since the cardinality constraint $ATLc$ cannot be satisfied.

5.2 Network degree

Here, we consider a fixed cardinality constraint $ATL1$, but the result would be qualitatively similar for any cardinality constraint.

Within each network class, Figure 6 shows the impact of the degree of the nodes on the resulting patterns. Clearly, whatever the network class, the higher the (mean) node degree, the higher the percentage of N positive cells. This is easily explained by the fact that a higher degree allows a single D positive cell to activate N in more neighbouring cells.

Furthermore, for non-regular networks, the wider the degree distribution (see Figure 3-A), the lower the percentage of N positive cells. However, beyond the degree, another characteristic must impact the resulting patterns, since the percentages of N positive cells differ within the class of regular networks. We propose in the next section that the number of shared neighbours may explain these differences.

5.3 Number of shared neighbours

Recall that, given a pair of connected nodes, their number of shared neighbours relates to their dissimilarity measure. Here, we consider the average number of shared neighbours, accounting for all pairs of connected nodes.

Although limited differences, a higher number of shared neighbours seems to lead to an increase of the percentages of N positive cells (see Figure 7). This can be informally explained as follows: two connected cells are either both N positive or of different types (Notch and Delta); in the first case, their shared neighbours can also be N positive (provided the presence of a D positive cell in the neighbourhood), whereas in the later case their shared neighbours are necessarily N positive cells.

From Figure 7, within the regular networks, it appears that when $k = 4$ (resp. $k = 6$) the percentage of N positive cells

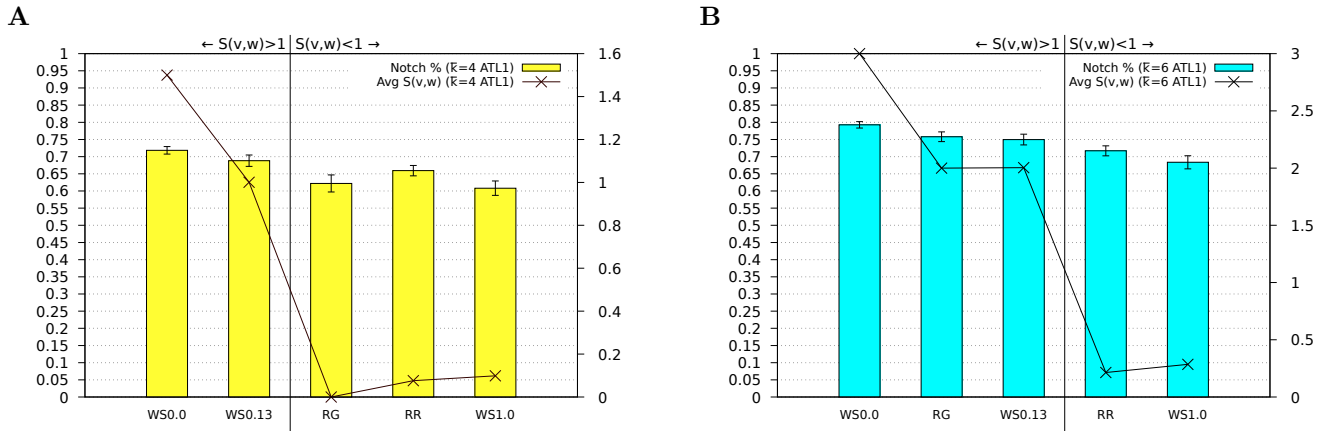

Fig. 7. Average percentages of N positive cells (left Y axis, bars) and average numbers of shared neighbours (right Y axis, marks) for each network class, with a cardinality constraint fixed to $ATL1$ and average degrees $\bar{k} = 4$ (A) and $\bar{k} = 6$ (B).

grows with the number of shared neighbours, *i.e.*, WS0.0 leads to more N positive cells than WS0.13, which leads to more N positive cells than RG (resp. WS0.0 leads to more N positive cells than RG, which leads to (slightly) more N positive cells than WS0.13). The same property holds for the (non-regular) Watts-Strogatz networks WS0.13 and WS1.0, where the former leads to a higher percentage of N positive cells and has a higher average number of shared neighbours (for both $\bar{k} = 4$ and $\bar{k} = 6$).

6. DISCUSSION AND CONCLUSION

Our goal was to assess the impact of the communication network underlying the EpiLog grid. To do so, we considered various classes of regular and non-regular networks and, focusing on the Notch signalling system, we evaluated the obtained stable patterns in terms of percentages of N positive cells. Overall, these percentages do not change drastically, suggesting that a 2D hexagonal grid (RG, $k = 6$) is a reasonable approximation for the modelling of simple epithelial tissues. However, we showed that the network topology does have a measurable impact, which depends on regularity, degree and average number of shared neighbours.

From Figure 5, it appears that the closest percentage of N positive cells is obtained with the WS0.13 ($\bar{k} = 6$) network. This network has a degree distribution quite similar to the one observed in nature (Gibson et al., 2006), and could be taken as a reference.

Network regularity matters in keeping a complementarity property between cardinality constraints, where percentages of N positive cells for complementary cardinality constraints, *e.g.* $ATL1$ and $ATL6$, add up to 100% (see Figure 5). This property is not maintained with non-regular communication networks, however the WS0.13 is the one which almost keep this complementarity.

Moreover, the numbers of shared neighbours seem to impact the resulting patterns (Figure 7). Here again, the WS0.13 network is the network whose number of shared neighbours is the closest to that of the RG.

The patterns reached with the Boolean Delta-Notch model used for this study were qualified by the percentage of N positive cells. This measure does not allow to assess the nature of the pattern in terms of local organisation, regularity and symmetry. In Palau-Ortin et al. (2015), the authors propose parameters that allow to do so. However, these parameters are defined for the hexagonal grid, and their extension to general communication networks might be difficult. Nonetheless, it would be interesting to have a measure that better qualify the organisation of the patterns resulting from the lateral-inhibition model for different communication networks.

Finally, we relied for this study on a simple lateral-inhibition model. The observations made with this model could be generalised for other patterning systems.

7. AVAILABILITY

Python scripts used to generate the communication networks for each network class, to extract the network characteristics, to perform the simulations with EpiLog, and to extract the Notch percentage from the obtained patterns is available at `http://epilog-tool.org/node/190`.

ACKNOWLEDGEMENTS

We would like to thank Alain Guénoche and Luís Correia for insightful discussions.

REFERENCES

Abou-Jaoudé, W., Traynard, P., Monteiro, P.T., Saez-Rodriguez, J., Helikar, T., Thieffry, D., and Chaouiya, C. (2016). Logical modeling and dynamical analysis of cellular networks. *Front Genet*, 7, 94. doi:10.3389/fgene.2016.00094.

Albert, R. and Othmer, H.G. (2003). The topology of the regulatory interactions predicts the expression pattern of the segment polarity genes in drosophila melanogaster. *Journal of Theoretical Biology*, 223(1), 1–18. doi:10.1016/s0022-5193(03)00035-3.

Angelelli, J.B., Baudot, A., Brun, C., and Guénoche, A. (2008). Two local dissimilarity measures for weighted graphs with application to protein interaction networks. *Advances in Data Analysis and Classification*, 2(1), 3–16. doi:10.1007/s11634-008-0018-3.

Azpeitia, E., Benítez, M., Vega, I., Villarreal, C., and Alvarez-Buylla, E.R. (2010). Single-cell and coupled grn models of cell patterning in the arabidopsis thaliana root stem cell niche. *BMC Systems Biology*, 4(1), 134. doi:10.1186/1752-0509-4-134.

Barrat, A. and Weigt, M. (2000). On the properties of small-world network models. *The European Physical Journal B - Condensed Matter and Complex Systems*, 13(3), 547–560. doi:10.1007/s100510050067.

Chaouiya, C., Lang, F., Batt, G., Mendes, N.D., Mateescu, R., and Le Cornec, Y.S. (2013). Composition and abstraction of logical regulatory modules: application to multicellular systems. *Bioinformatics*, 29(6), 749–757. doi:10.1093/bioinformatics/btt033.

Collier, J.R., Monk, N.A.M., Maini, P.K., and Lewis, J.H. (1996). Pattern formation by lateral inhibition with feedback: a mathematical model of delta-notch intercellular signalling. *Journal of Theoretical Biology*, 183(4), 429–446. doi:10.1006/jtbi.1996.0233.

Fatès, N. (2013). A guided tour of asynchronous cellular automata. In *Cellular Automata and Discrete Complex Systems*, 15–30. Springer Berlin Heidelberg. doi:10.1007/978-3-642-40867-0_2.

Fauré, A., Vreede, B.M.I., Sucena, E., and Chaouiya, C. (2014). A discrete model of drosophila eggshell patterning reveals cell-autonomous and juxtacrine effects. *PLoS Comput Biol*, 10(3), e1003527. doi:10.1371/journal.pcbi.1003527.

Ghosh, R. and Tomlin, C. (2004). Symbolic reachable set computation of piecewise affine hybrid automata and its application to biological modelling: Delta-notch protein signalling. *Systems Biology*, 1, 170–183(13).

Gibson, M.C., Patel, A.B., Nagpal, R., and Perrimon, N. (2006). The emergence of geometric order in proliferating metazoan epithelia. *Nature*, 442, 1038 EP –. doi:10.1038/nature05014.

Hagberg, A.A., Schult, D.A., and Swart, P.J. (2008). Exploring network structure, dynamics, and function using NetworkX. In G. Varoquaux, T. Vaught, and J. Millman (eds.), *Proceedings of the 7th Python in Science Conference*, 11 – 15. Pasadena, CA USA.

Matsuda, M., Koga, M., Woltjen, K., Nishida, E., and Ebisuya, M. (2015). Synthetic lateral inhibition governs cell-type bifurcation with robust ratios. *Nature Communications*, 6(1). doi:10.1038/ncomms7195.

Palau-Ortin, D., Formosa-Jordan, P., Sancho, J., and Ibañes, M. (2015). Pattern selection by dynamical biochemical signals. *Biophysical Journal*, 108(6), 1555–1565. doi:10.1016/j.bpj.2014.12.058.

Sánchez, L., Chaouiya, C., and Thieffry, D. (2008). Segmenting the fly embryo: logical analysis of the role of the segment polarity cross-regulatory module. *Int J Dev Biol*, 52(8), 1059–75. doi:10.1387/ijdb.072439ls.

Steger, A. and Wormald, N.C. (1999). Generating random regular graphs quickly. *Combinatorics, Probability and Computing*, 8(4), 377396.

Tonello, E. and Siebert, H. (2019). Boolean analysis of lateral inhibition.

Varela, P.L., Lynce, I., Manquinho, V., Chaouiya, C., and Monteiro, P.T. (2018a). Stable states of boolean regulatory networks composed over hexagonal grids. *Electronic Notes in Theoretical Computer Science*, 335, 113–130. doi:10.1016/j.entcs.2018.03.011.

Varela, P.L., Ramos, C.V., Monteiro, P.T., and Chaouiya, C. (2018b). EpiLog: A software for the logical modelling of epithelial dynamics. *F1000Res*, 7, 1145. doi:10.12688/f1000research.15613.1.

Vetter, R., Kokic, M., Gómez, H., Hodel, L., Gjeta, B., Iannini, A., Villa-Fombuena, G., Casares, F., and Iber, D. (2019). Aboave-weaire's law in epithelia results from an angle constraint in contiguous polygonal lattices. *bioRxiv*. doi:10.1101/591461.

Watts, D.J. and Strogatz, S.H. (1998). Collective dynamics of 'small-world' networks. *Nature*, 393(6684), 440–442. doi:10.1038/30918.